Long-term Cultures of Bone Marrow–Derived Human Mesenchymal Stem Cells Frequently Undergo Spontaneous Malignant Transformation

Gro Vatne Røsland,[1] Agnete Svendsen,[1] Anja Torsvik,[1] Ewa Sobala,[7] Emmet McCormack,[2] Heike Immervoll,[3,5] Josef Mysliwietz,[8] Joerg-Christian Tonn,[7] Roland Goldbrunner,[7] Per Eystein Lønning,[4,6] Rolf Bjerkvig,[1,9] and Christian Schichor[7]

Department of [1]Biomedicine, [2]Hematology Section, Department of Medicine, [3]Section of Pathology, The Gade Institute, and [4]Section of Oncology, Institute of Medicine, University of Bergen; Departments of [5]Pathology and [6]Oncology, Haukeland University Hospital, Bergen, Norway; [7]Neuro-oncological Laboratory, Department of Neurosurgery, Ludwigs-Maximilians-University; [8]Institute for Molecular Immunology, National Research Center for Environment and Health, Munich, Germany; and [9]NorLux Neuro-Oncology, Centre Recherche de Public Santé, Luxembourg

Abstract

Human mesenchymal stem cells (hMSC) aid in tissue maintenance and repair by differentiating into specialized cell types. Due to this ability, hMSC are currently being evaluated for cell-based therapies of tissue injury and degenerative diseases. However, extensive expansion *ex vivo* is a prerequisite to obtain the cell numbers required for human cell-based therapy protocols. Recent studies indicate that hMSC may contribute to cancer development and progression either by acting as cancer-initiating cells or through interactions with stromal elements. If spontaneous transformation *ex vivo* occurs, this may jeopardize the use of hMSC as therapeutic tools. Whereas murine MSC readily undergo spontaneous transformation, there are conflicting reports about spontaneous transformation of hMSC. We have addressed this controversy in a two-center study by growing bone marrow–derived hMSC in long-term cultures (5–106 weeks). We report for the first time spontaneous malignant transformation to occur in 45.8% (11 of 24) of these cultures. In comparison with hMSC, the transformed mesenchymal cells (TMC) showed a significantly increased proliferation rate and altered morphology and phenotype. In contrast to hMSC, TMC grew well in soft agar assays and were unable to undergo complete differentiation. Importantly, TMC were highly tumorigenic, causing multiple fast-growing lung deposits when injected into immunodeficient mice. We conclude that spontaneous malignant transformation may represent a biohazard in long-term *ex vivo* expansion of hMSC. On the other hand, this spontaneous transformation process may represent a unique model for studying molecular pathways initiating malignant transformation of hMSC. [Cancer Res 2009;69(13):5331–9]

Introduction

Multipotent mesenchymal stem cells may differentiate into various cell lineages including osteoblasts, tenocytes, adipocytes, chondrocytes, myoblasts, and even neurons (1). Thus, these cells are considered to be promising tools for cell-targeted therapies and tissue engineering (2, 3). Tissue-specific human mesenchymal stem cells (hMSC) can be harvested from multiple sources, including placental tissue (4), amniotic fluid (5), cord blood (6), and adipose tissue (7). Yet, bone marrow aspirations remain the hMSC source of choice in most laboratories (8). However, to obtain sufficient cell numbers for clinical protocols, extensive *ex vivo* expansion is required. Recent controversies about the stability of hMSC (9–12) highlight the need to address hMSC stability in long-term cultures before clinical use.

Although stem cells were identified as precursors of hematologic malignancies more than a decade ago (13), stem cells have only recently been identified as cancer-initiating cells in solid malignancies (14–17). Moreover, whether most solid tumor–initiating cells derive from undifferentiated precursor cells or undifferentiated cells may play an important role in carcinogenesis by interactions with the tumor stroma is not fully understood (18). Albeit MSC are considered precursors of mesenchymal-derived solid tumors, such as sarcomas (19), their role in carcinogenesis may go beyond that. Thus, Houghton and colleagues (20) showed MSC to home from their bone marrow residence, progressing into gastric carcinomas in response to *Helicobacter felis* infection in mice.

Spontaneous transformation of murine MSC has been observed by others (21, 22), although conflicting evidence suggests this may not be the case for hMSC. Studies indicating no spontaneous transformation in long-term hMSC cultures have been reported (9, 10). However, one group observed spontaneous malignant transformation of adipose-derived hMSC *in vitro* (11), whereas another group reported a transformed population arising in one culture of bone marrow–derived hMSC/CD133$^+$ (12). In accordance with the findings by Rubio and colleagues (11) about genomic instability in transformed mesenchymal cells (TMC), we suggested genomic plasticity of undifferentiated hMSC to permit longevity and thereby render the cells particularly prone to malignant transformation. Accumulation of DNA damage through genomic instability, loss of cell cycle regulation, and deregulated epigenetic signature may arise during long-term culture under standard *in vitro* conditions, and eventually result in malignant transformation.

The purpose of this study was to evaluate the risk of spontaneous malignant transformation of bone marrow–derived hMSC *in vitro.* Our findings reveal that 11 of 24 hMSC cultures underwent spontaneous transformation, resulting in highly malignant cells with an aggressive metastatic propensity in nonobese diabetic/severe combined immunodeficient (NOD/SCID) mice. Whereas our findings have significant implications with respect to hMSC *ex vivo*

Note: G.V. Røsland, A. Svendsen, and A. Torsvik contributed equally to this work.

Requests for reprints: Rolf Bjerkvig, Department of Biomedicine, University of Bergen, Jonas Lies vei 91, N-5009 Bergen, Norway. Phone: 47-55-58-63-52; Fax: 47-55-58-63-60; E-mail: rolf.bjerkvig@biomed.uib.no.

doi:10.1158/0008-5472.CAN-08-4630

biohazards, it also reveals a unique model to study spontaneous malignant transformation in stem cells.

Materials and Methods

Isolation and culture of bone marrow–derived hMSC. After obtaining written informed consent, bone marrow aspirates were collected from 24 healthy donors (14 from Bergen, Norway and 10 from Munich, Germany) and cultured according to two previously reported protocols (23, 24). Age of donors ranged from 18 to 53 y. The mononuclear cell fractions were isolated by Lymphoprep density gradient centrifugation (1.077 g/mL; Axis-Shield) at 800 × *g* for 25 min. The cells were washed and plated at $1 \times 10^6/25$ cm^2 in tissue culture flasks (Nunc). Marrow stromal cells were selected by plastic adherence. Stromal cell cultures were passaged on reaching subconfluence or within 6 to 8 d using 0.25% trypsin and 1 mmol/L EDTA, and replated at medium densities (6,000 cells/cm^2). The cells were cultured at 37°C in 5% CO_2 and 21% O_2 in medium containing α-modified MEM or DMEM supplemented with 2 mmol/L glutamine, 100 units/mL penicillin, 0.1 mg/mL streptomycin, and 10% fetal bovine serum (FBS). Unless otherwise stated, all cell culture products were purchased from Sigma-Aldrich. Phenotypic changes were examined microscopically every second day.

Phenotypic characterization by flow cytometric analysis. Briefly, 5×10^5 cells were analyzed for expression of the following surface markers (see Table 1 for further characteristics): rabbit anti–platelet endothelial cell adhesion molecule-1 (CD31; 1:20; Santa Cruz Biotechnology), mouse anti-CD34-FITC (1:40; Southern Biotech), mouse anti–homing-associated cell adhesion molecule (CD44; 1:20; Sigma-Aldrich), mouse anti-CD45-FITC (1:24; Southern Biotech), mouse anti-SH2/SH3 (CD73; 1:50; BD Biosciences), mouse anti–Thy-1 (CD90)-FITC (1:12; Chemicon), mouse anti-endoglin (CD105)-R-PE (1:40; Southern Biotech), mouse anti–activated leukocyte cell adhesion molecule (CD166; 1:50; BD Biosciences), mouse anti–Stro-1 (1:18; this monoclonal antibody, developed by Beverly Torok-Storb, was obtained from the Developmental Studies Hybridoma Bank, developed under the auspices of the National Institute of Child Health and Human Resources and maintained by The University of Iowa, Department of Biological Sciences, Iowa City, IA), mouse anti–HLA-I FITC (1:10; RayBiotech), and mouse anti–HLA-DR FITC (1:40; Southern Biotech). Cells (10^6) were analyzed for rabbit anti–α-smooth muscle actin (ASMA; 1:20; Abcam) using LEUCOperm (AbD; Serotec) for intracellular antigen staining. FITC-goat anti-mouse IgG (1:100; Immunotech SAS), FITC-goat anti-rabbit immunoglobulin (1:300; Southern Biotech), FITC-goat anti-mouse IgG1 (1:300; Southern Biotech), and FITC-rat anti-mouse IgM (1:100; eBioscience) were used for detection of unconjugated primary antibodies. Ten thousand cells were analyzed on a FACSCalibur (BD Biosciences) using the proper controls to set gates. Samples before and after transformation were compared using WinMDI software (The Scripps Research Institute, Flow Cytometry Core Facility).

Multilineage differentiation potential of hMSC. Adipogenic, chondrogenic, and osteogenic differentiation assays (Differentiation media Bullet Kits, Cambrex) were done on hMSC and TMC according to the manufacturer's instructions. The extent of adipogenic induction was verified by fixation in 10% buffered formalin and staining of lipid vacuoles in 0.5% Oil-Red-O. Chondrogenic induction was verified by morphologic examination of H&E on paraffin sections and collagen type IV immunohistochemistry (1:250; Sigma-Aldrich), visualized by EnVision-HRP DAB System protocol (DakoCytomation). Osteogenic induction was verified by a

Table 1. Characteristics of selected cell surface markers

Common name	CD locus	Specificity	Selected functions	Reference
PECAM-1	CD31	Platelet/endothelial cell adhesion molecule	Cell-cell interactions during growth and development	(40)
	CD34	2–4% of bone marrow cells, including HSC, endothelial cells, a subset of fibroblasts, and tumor cells	Adhesion and signal transduction through PKC	(41)
HCAM	CD44	Peripheral blood leukocytes, RBC, bone marrow nucleated cells, fibroblasts, and others	Cell-cell and cell-matrix interactions	(42)
Leukocyte common antigen	CD45	WBC	Regulator of T-cell signaling	(43)
SH2/SH3	CD73	CFU-F present in human bone marrow, subset of lymphocytes, epithelial, and endothelial cells	Catalyzes dephosphorylation of AMP	(44)
Thy-1	CD90	Thymocytes, hMSC, peripheral and some intraepithelial T lymphocytes, and neurons	T-cell activation, apoptosis, tumor suppression, fibrosis	(45)
Endoglin	CD105	Endothelial cells	Receptor for transforming growth factor β	(46)
ALCAM	CD166	Neurons, activated T cells and monocytes, epithelial cells, and fibroblasts	Cell-cell interactions	(47)
Stro-1 (stromal cell precursor 1)	—	Mesenchymal precursor cells	Unknown	(48)
ASMA	—	α-Smooth muscle actin/smooth muscle cells	A major constituent of the contractile apparatus	(49)
HLA-1	—	Class I MHC complex, expressed on nucleated cells	Presentation of peptides from endogenous proteins	(50)
HLA-DR	—	Class II MHC complex on B cells, T cells, monocytes, macrophages, and APC	Presentation of peptides to $CD4^+$ T lymphocytes	(50)

Abbreviations: PECAM-1, platelet endothelial cell adhesion molecule 1; ALCAM, activated leukocyte cell adhesion molecule; HCAM, homing-associated cell adhesion molecule; HSC, hematopoietic stem cells; PKC, protein kinase C; APC, antigen-presenting cells.

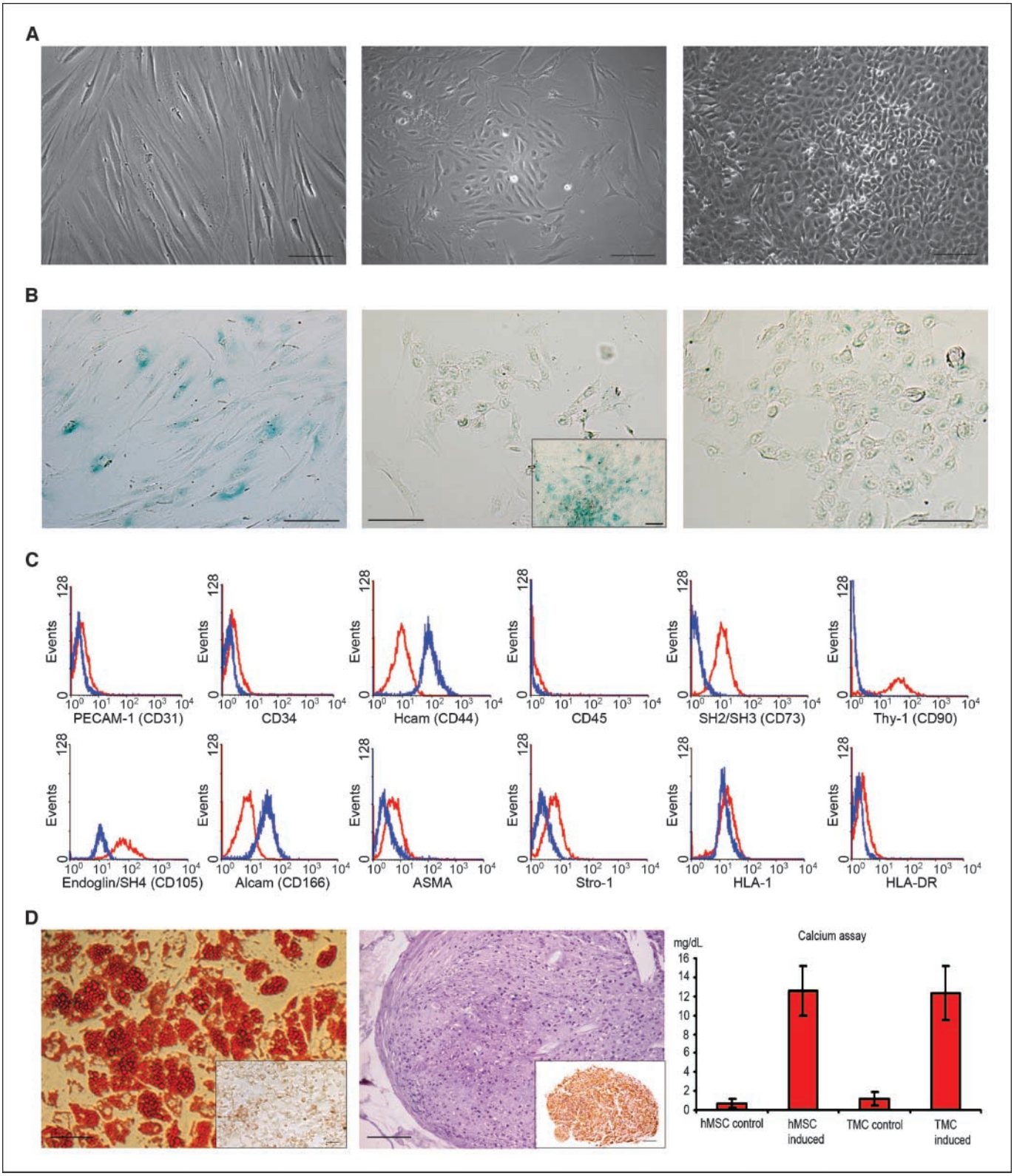

Figure 1. Spontaneous malignant transformation of hMSC. *A,* morphologic changes during (*middle*) and after (*right*) malignant transformation, in comparison with hMSC (*left*). *Bar,* 125 μm. *B,* increased senescence-assosiated β-galactosidase activity observed in hMSC entering senescence (*left*), as well as cells escaping senescence during malignant transformation (*middle*). Senescence was not observed in TMC (*right*). *Bar,* 90 μm. *C,* a panel of CD markers describing altered expression of cell surface antigens in hMSC (*red*) versus TMC (*blue*). *D,* differentiation potential in hMSC versus TMC. Adipocytes derived from hMSC (*left*; *bar,* 90 μm). TMC cannot differentiate into adipose tissue (*left inset*; *bar,* 100 μm). Chondrocyte spheroides derived from hMSC, shown by H&E staining (*middle*; *bar,* 225 μm), as well as collagen IV assay (*middle inset*; *bar,* 360 μm). Calcium assay shows significantly increased production of calcium in hMSC and TMC ($P < 0.05$), indicating that both the hMSC and the TMC have a potential for differentiating into osteocytes (*right*). *PECAM-1,* platelet endothelial cell adhesion molecule-1; *ALCAM,* activated leukocyte cell adhesion molecule; *HCAM,* homing-associated cell adhesion molecule.

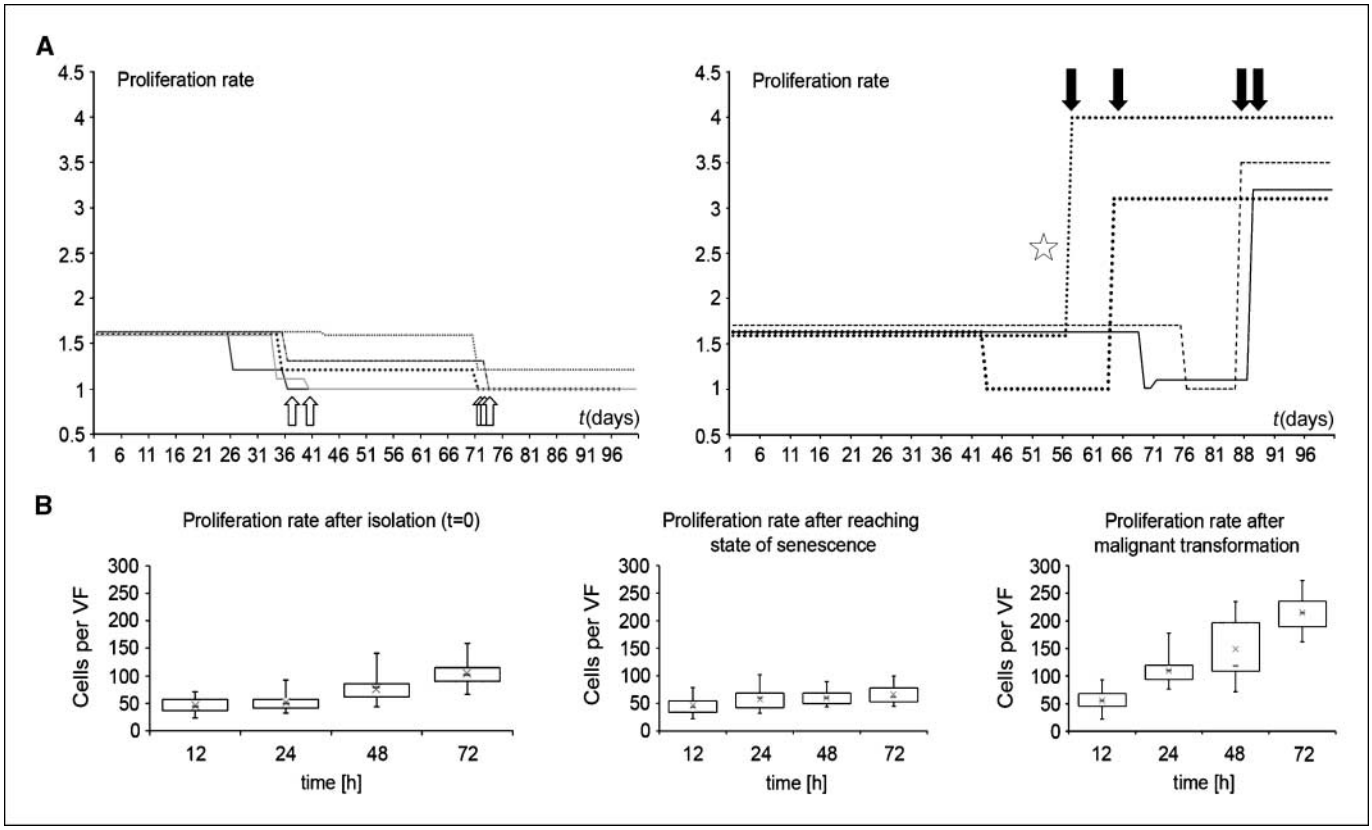

Figure 2. Increased proliferation rate after malignant transformation. *A,* proliferation rate of cultures that did not undergo malignant transformation (*left*) versus cultures that transformed into TMC (*right*). *Left,* arrows indicate the time point for entering senescence. Proliferation rates without significant changes are given as constant values over time (means). *Right,* arrows indicate time point for the onset of enhanced proliferation rate. In all but one sample (*asterisk*), the malignant transformation was preceded by detectable senescence. *B,* mean proliferation rate of hMSC after isolation (*left*), in the state of senescence (*middle*), and in spontaneously malignant transformed cells (*right*); *bars,* SD. After 48 h in culture, the proliferation rate increased significantly for TMC compared with hMSC after isolation ($P = 0.006$) and for TMC compared with senescent hMSC ($P = 0.002$). *VF,* visual field.

calcium deposition assay according to the Stanbio Total Calcium LiquiColor procedure (Stanbio Laboratories).

Proliferation assay. Proliferation assay was done as described elsewhere, with minor variations (25). Briefly, every 7 d, 6,000 cells were seeded in 24-well plates and counted after 12, 24, 48, and 72 h under an inverse microscope using 10 nonoverlapping visual fields per well. Four wells were counted for each donor. Statistics were done using Analyze-it software for Microsoft Excel.

Senescence-associated β-galactosidase staining. Increased endogenous β-galactosidase activity at pH 6 was used to determine the state of senescence according to the β-galactosidase assay protocol (Cell Signaling Technology). Examination by light microscopy confirmed the characteristic blue product in cells possessing high β-galacosidase activity.

Colony-forming assay. Colony-forming assay was done as previously described (26). Briefly, 1×10^5 single cells in suspension were seeded on an interface of two different Matrigel concentrations. Single-cell suspension was confirmed by microscopy. After 3 weeks of incubation, colony formations (diameter >60 μm) in the different specimens were compared. During long-term experiments, this setup was done repeatedly every week.

PCR. Total RNA was isolated from cultured cells using the RNeasy kit (Qiagen). cDNA synthesis was done with a cDNA kit (Boehringer) according to the manufacturer's protocol. PCR was done as previously described (1). The PCR products were analyzed using 2% agarose gel electrophoresis and visualized using ethidium bromide staining. The following oligonucleotide sequences were used: glyceraldehyde-3-phosphate dehydrogenase primers, 5′-TCCAAAATCAAGTGGGGCGATGCT-3′ (upper), 5′-ACCACCTGGTGCTCAGTGTAGCCC-3′ (lower); *hTERT* primers; 5′-ACCAAGCATTCCTGCTCAAGCTG-3′ (upper), 5′-CGGCAGGTGTGCTGGACACTC-3′ (lower).

Telomeric repeat amplification protocol (TRAP). Telomerase activity was measured using the Quantitative Telomerase Detection Kit (Allied Biotech) according to the manufacturer's protocol. Cell lysates were prepared using the TRAPEZE 1× CHAPS Lysis Buffer (Chemicon). The protein concentration for each lysate was determined using the Bio-Rad Protein Assay Kit. The samples were analyzed using an iCycler (Bio-Rad) and compared with a control template standard curve for final quantification of telomerase activity.

Lentiviral vector production and transduction. The lentiviral transfer vectors pWPXL-eGFP and pWPXL-LacZ, packaging plasmid psPAX.2, and envelope plasmid pMD2.G were kindly provided by Dr. Didier Trono's laboratory (CMU, Geneva, Switzerland). Lentiviral particles were produced according to the protocols described by Dr. Trono's lab.[10] Briefly, Superfect (Invitrogen) was used to triple-transfect psPAX.2, pMD2.G, and the respective transfer vectors into 293FT producer cells. Supernatant containing lentiviral particles was harvested 48 h posttransfection. TMC were transduced with lentiviral particles in the presence of 10 μg/mL polybrene (Sigma-Aldrich).

Fluorescence-activated cell sorting. For use in optical imaging experiments, lentivirally transduced cells harboring high enhanced green fluorescent protein (eGFP) expression were sorted using FACSAria Special Order Cell Sorting Instrument (Becton Dickinson) on the basis of single-cell viability and high eGFP expression. The fluorescence-activated cell sorting experiments were done at the Molecular Imaging Center (Fuge, Norwegian Research Council), University of Bergen.

***In vivo* experiments.** Immunodeficient NOD.CB17.Prkdc^{scid} mice (abbreviated NOD/SCID) from the Jackson Laboratory were used. The

[10] http://tronolab.epfl.ch

mice were anesthetized by 1% isofluorane and injected i.v. with 3.2×10^6 TMC or TMC-LacZ, or s.c. with 4.5×10^6 TMC in 250 μL physiologic saline. Control animals were injected with equal numbers of hMSC. Each group consisted of seven animals. The mice were monitored and weighed daily throughout the experiment. As soon as the animals lost 10% body weight or showed any signs of tumor burden, they were sacrificed and perfusion fixed with 3.7% paraformaldehyde before the tumors were removed and postfixed in 3.7% paraformaldehyde for 48 h. Tumors were embedded in paraffin, sectioned, and stained with H&E before examination by microscopy. All experiments were approved by The Norwegian Animal Research Authority and conducted according to The European Convention for the Protection of Vertebrates Used for Scientific Purposes.

***In vivo* optical imaging.** NOD/LtSz-*Prkdc*^{scid}/*B2m*^{null} (27) mice (abbreviated as NOD/SCID/β2m^{null}; originally obtained from Dr. Leonard Schultz, The Jackson Laboratory, Bar Harbor, ME) were expanded and maintained under defined flora conditions in individually ventilated (HEPA-filtered air) sterile microisolator cages (Techniplast) at the University of Bergen animal facility. Before imaging, anesthetized mice were depilated and moved to the heated translational stage of the eXpore Optix (ART/GE Healthcare). Animals were maintained under gas anesthesia during scanning.

TMC-eGFP *in vivo* model. NOD/SCID/β2m^{null} mice, 6 to 8 wk old ($n = 7$ per group), were irradiated from a photon radiation source (BCC Dynaray CH4, 4-MV photon irradiation source) with a sublethal dose of 2.5 Gy (60 cGy/min) 24 h before injection. TMC-eGFP or hMSC (3×10^6) were suspended in 200 μL physiologic saline before injection via the dorsal tail vein. Recipient mice were monitored every second day by time-domain optical imaging for eGFP and sacrificed following institutional guidelines when moribund, as defined by weight loss, lethargy, and/or paralysis/respiratory distress.

Time-domain fluorescence imaging. For eGFP fluorescence imaging, we used an eXplore Optix time-domain imager configured for eGFP imaging experiments as previously described (28). For *in vivo* studies, whole-body images of mice were taken before TMC inoculation and used as representative background autofluorescence for every animal. Subsequently, raw fluorescence data were analyzed by fitting of measured fluorescence lifetime decay signal by the Levenberg Marquet least squares method (28) and fluorescence lifetime gating for eGFP (2.65 ns) using Optiview software (ART, Advanced Research Technologies, Inc.).

Immunohistochemistry. Immunohistochemical staining was done on 5-μm paraffin sections of tumor tissue. Sections on coated glass slides were dried 1 h at 60°C; all subsequent steps were done at room temperature. Retrieval method, buffer solutions, antibody detection method, and concentration of the primary antibodies were varied according to the protocols described for each primary antibody. The following antibodies were used: pan-cytokeratin AE1/AE3 (1:100; DakoCytomation), CK18 DC10 [1:100; Lab Vision (Neomarkers)], CK13 KS-1A3 (1:400; Novocastra), vimentin V9 (1:100; DakoCytomation), actin 1A4 (1:600; DakoCytomation), and CD99 12E7 (1:400; DakoCytomation). The slides were incubated with primary antibody for 60 min at room temperature. Unspecific peroxidase activity was blocked by 3% H_2O_2 treatment for 5 min. The signal was developed with diaminobenzidine DAB$^+$ (DakoCytomation) for 5 min. Between each step, there were two 1-min washing steps in washing buffer (15 mmol/L Tris, 5 mmol/L NaCl, 0.05% Tween 20; pH 7.5). Finally, the slides were counterstained with hematoxylin for 1 min, dehydrated, and mounted in Entellan (Merck). For microscopy, a Leica DMLB microscope was used. Pictures were taken with ColorView soft imaging system (Olympus).

Fluorescence *in situ* hybridization on paraffin-embedded TMC tumors in mice. *Pretreatment and hybridization:* Tissue sections of s.c. TMC tumors were deparaffinized and rehydrated. The samples were pretreated using a Histology FISH Accessory Kit (DakoCytomation) following the manufacturer's description. The slides were treated with 0.2 mg/mL RNase A (Sigma-Aldrich) in 2× SSC (3 mol/L NaCl, 0.3 mol/L sodium citrate, pH 7.0) for 15 min at 37°C and washed 3 × 2 min in PBS/0.2% Tween. The slides were dehydrated and air-dried. A mixture of probes, Star*FISH Human Chromosome Pan-Centromeric Probes FITC labeled and Star*FISH Mouse Pan-Centromeric Probes Cy3 labeled (Cambio), was preheated at 70°C for 5 min and cooled to 37°C. The probe was applied to the tumor sections and sealed using CISH UnderCover-Slips (Invitrogen). The slides were hybridized for 1 d on a Techne Flexigene Thermal Cycler at 90°C 8 min, 80°C 1 min, 60°C 1 min, 45°C 4 h, 42°C 4 h, and 37°C overnight. *Stringency wash and mounting:* Probe was rinsed off using distilled water and PBS. The slides were immersed and washed 2 × 10 min in 2× SSC, 2 × 5 min in PBS/0.2% Tween, and mounted with Vectashield with 4′,6-diamidino-2-phenylindole DAPI (Vector Labs). The samples were examined by a Leica DM RXA fluorescence microscope (Leica Microsystems).

Results and Discussion

Rate of spontaneous malignant transformation in hMSC cultures. To address the current controversies about spontaneous malignant transformation of hMSC cultures, bone marrow–derived hMSC samples were harvested and expanded in two different laboratories. Following long-term hMSC culture *in vitro*, we observed spontaneous malignant transformation in 11 of 24 (45.8%) cultures. The rate of transformation in the two separate laboratories was 50% (7 of 14) and 40% (4 of 10), respectively. The transformation was characterized by dramatically altered morphology, from uniform spindle-shaped cells (hMSC; Fig. 1*A, left*) to round epithelial-like cells displaying an increased nucleus-to-cytoplasma ratio (Fig. 1*A, right*). Transformed cells arose in colonies (Fig. 1*A, middle*), indicating clonal origin of the transformed cells. Notably, 8% (2 of 24) of the cultures transformed without preceding signs of senescence. In the remaining samples (41%, 9 of 22), the changes in morphology occurred after a phase of senescence, as determined

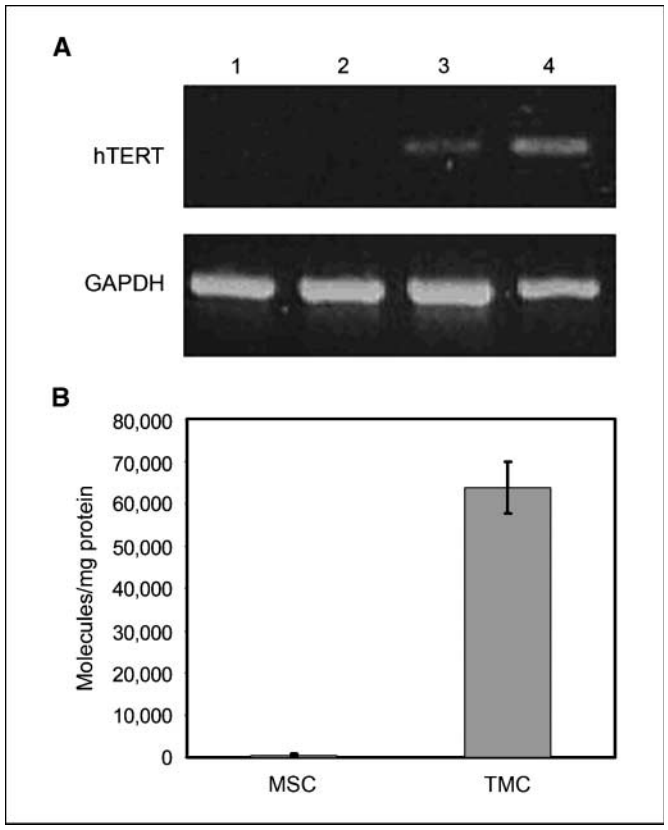

Figure 3. Up-regulation of telomerase activity. *A,* reverse transcription-PCR revealing overexpression of *hTERT* in TMC (*lanes 3* and *4*) compared with hMSC (*lanes 1* and *2*, respectively). *GAPDH,* glyceraldehyde-3-phosphate dehydrogenase. *B,* telomerase activity increased significantly in TMC compared with hMSC ($P = 0.00003$), as measured by TRAP assay. For hMSC, the calculated mean value of telomerase was 520 ± 288 molecules/mg total protein, whereas the mean value of TMC was 63,800 ± 6,013 molecules/mg protein.

by decreased proliferation and senescence-associated β-galactosidase staining at pH 6 (Fig. 1*B*). These findings indicate that escape from senescence is a crucial step in the malignant transformation for the majority of samples.

To determine the influence of soluble factors in various serum, we have tested fetal bovine serum purchased from Biochrom, Sigma-Aldrich, and Biowest. The different sera were not found to influence the frequency of transformation (data not shown). Commercially available media for hMSC culture, Mesencult (Stem Cell Technologies) and MSCBM (Cambrex), were also tested, and malignant transformation was found to occur in samples cultured with these media at a frequency similar to noncommercial media. To determine whether TMC-derived paracrine factors may favor transformation, we also grew hMSC in conditioned medium obtained from TMC. We did not observe any induction of transformation (data not shown). Taken together, the results from our study indicate that malignant transformation is not triggered solely by contents of the cell culture medium or cell-derived paracrine factors, but rather suggest that intrinsic properties of hMSC may drive the process of malignant transformation.

Phenotypic alterations of TMC. To characterize the phenotypic differences between hMSC and TMC, the cultures were assayed by immunocytochemistry and analyzed by multicolor flow cytometry. Bone marrow–derived hMSC expressed high levels of the cell surface markers CD73, CD90, CD105, and HLA-1 and moderate levels of CD44, CD166, ASMA, and Stro-1. In addition, bone marrow–derived hMSC did not express the following cell surface markers: CD31, CD34, CD45, and HLA-DR (Fig. 1*C, red*). These observations are in line with recently published phenotypic expression patterns of hMSC (29, 30). Compared with hMSC, TMC showed increased expression of CD44 and CD166, whereas CD105 was slightly downregulated. Some markers used to identify hMSC, such as CD73, CD90, ASMA, and Stro-1, were undetectable in TMC (Fig. 1*C, blue*).

Limited differentiation potential of TMC. Human MSC cultured in the appropriate differentiation media caused differentiation into adipocytes, chondrocytes, and osteocytes (Fig. 1*D*). After transformation, the potential of cells to differentiate into adipocytes and chodrocytes was dramatically reduced (Fig. 1*D, left inset*; and data not shown). However, differentiation into the osteogenic lineage induced elevated calcium production in TMC similar to hMSC (Fig. 1*D, right*), indicating intact osteogenic differentiation potential in TMC. The possible application of differentiation induction in a therapeutic context of sarcomas should therefore be further explored.

Senescence precedes malignant transformation in the majority of cultures. With exception of the two hMSC samples where no signs of senescence were detected before malignant transformation, all hMSC cultures entered senescence 25 to 71 days after harvest and initial seeding, represented by β-galactosidase staining (Fig. 1*B*), as well as decreased proliferation rate (Fig. 2). In contrast to the fast proliferating hMSC cultures with a mean cell doubling time of 60 hours during the first 6 to 10 weeks after harvest (Fig. 2*B, left*), the senescent cultures had a mean cell doubling time of 214 hours (Fig. 2*B, middle*). Among the senescent cultures, 41% (9 of 22) escaped senescence and underwent malignant transformation. TMC displayed a mean doubling time of only 12 hours (Fig. 2*B, right*). On escape from senescence, the TMC cultures were immortalized, and at present, the TMC are still in continuous culture and have exceeded more than 100 passages.

Transformation causes an increase in telomerase activity. Telomerase is activated in 70% to 90% of malignant tissues (31) and

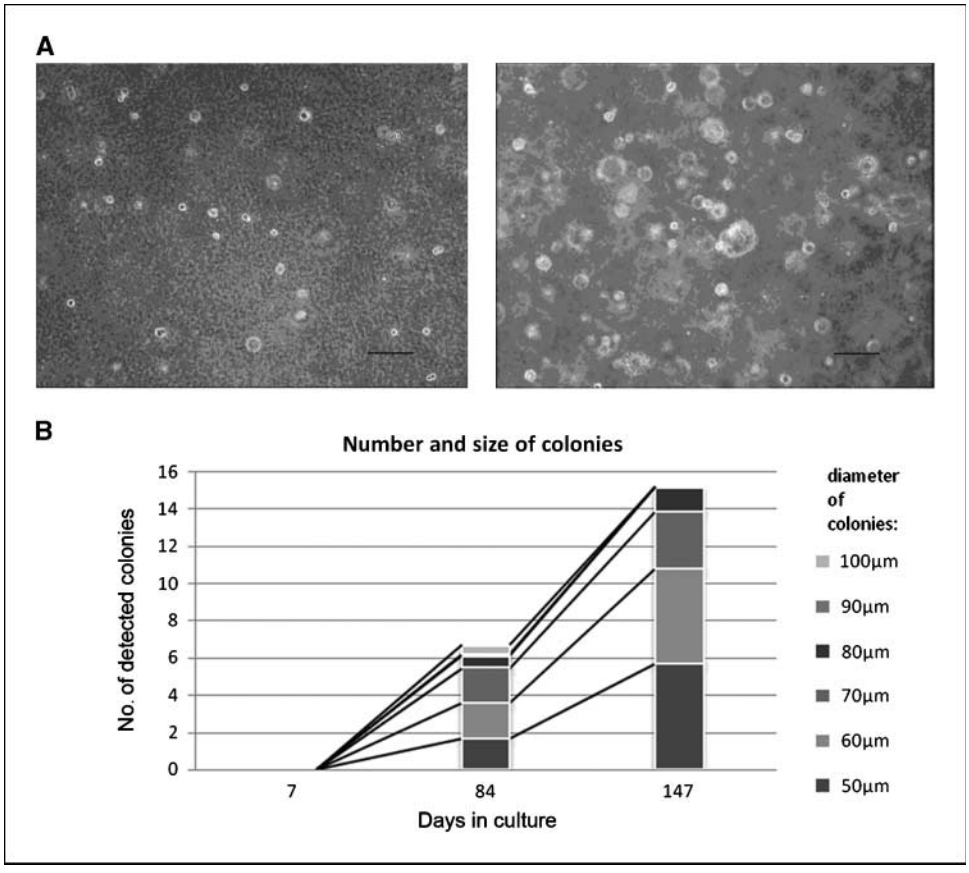

Figure 4. Enhanced colony formation of malignant transformed hMSC *in vitro*. *A,* hMSC after isolation (*left*) and TMC after malignant transformation (*right*). Pictures were taken 21 d after initial seeding. *Bar,* 200 μm. *B,* quantification of anchorage-independent growth in colonies. No colonies could be detected after isolation (day 7); multiple colonies were seen after transformation (day 84). The number as well as the size of colonies increased during further culturing (day 147).

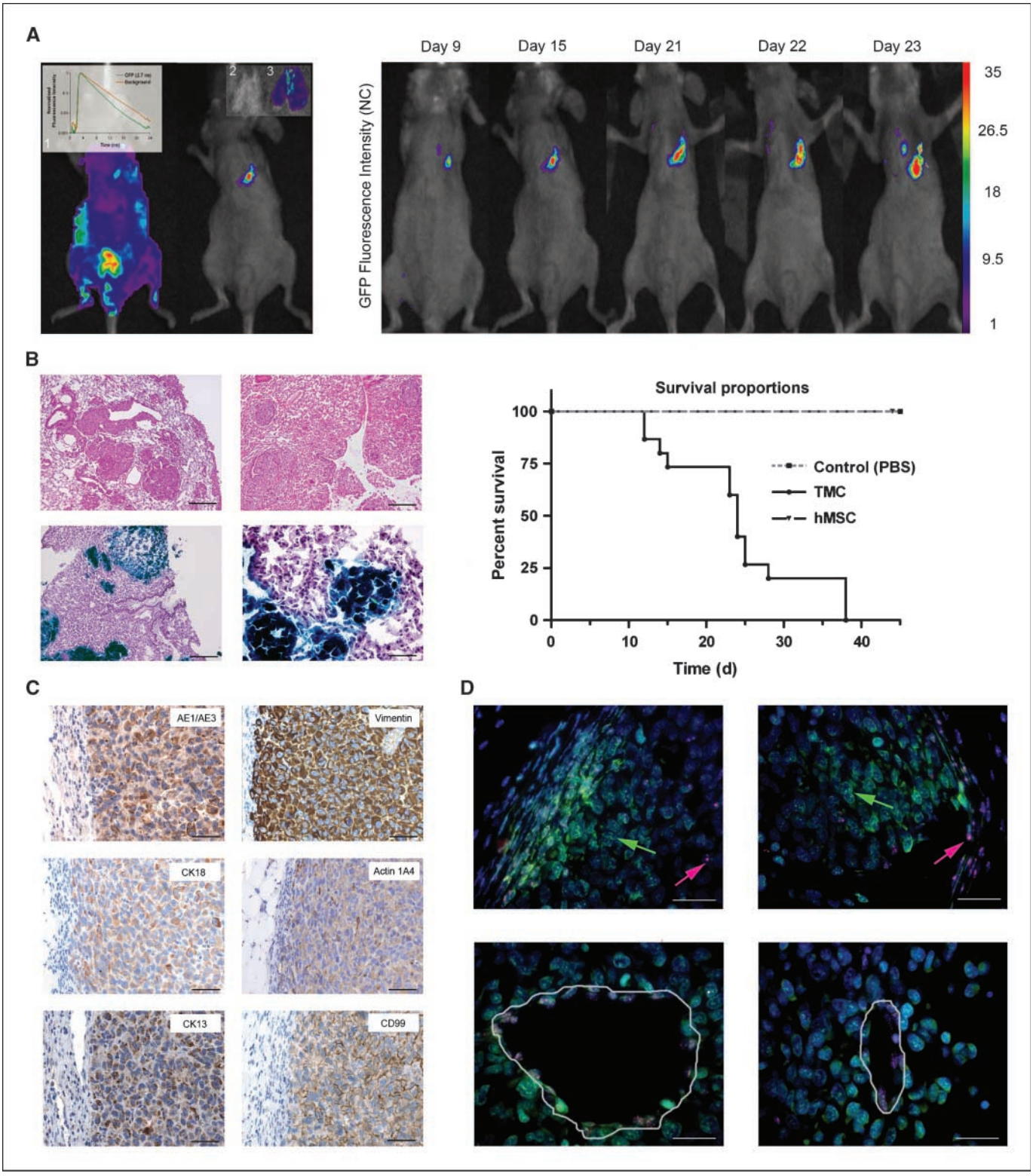

Figure 5. TMC are tumorigenic *in vivo. A, left,* raw fluorescence intensity image acquired by time-domain imaging 15 d after inoculation of 3×10^6 TMC-eGFP. By gating whole-body images for the fluorescence lifetime of eGFP, the fluorescence resultant of TMC-eGFP could be determined (*inset 1*). The fluorescence intensity of TMC-eGFP was predominantly seen in the lungs. Necropsy of the lungs verified accumulation of signal in the TMC-eGFP mice (*inset 3*) versus hMSC control mice (*inset 2*). *Right,* increasing eGFP signal could be detected over time *NC,* normalized counts. *B, left,* H&E staining confirmed the infiltrative tumor phenotype following i.v. injection of TMC (*top left*; *bar,* 500 μm) and s.c. injection (*top right*; *bar,* 300 μm). I.v. injection of TMC-LacZ confirmed the human xenograft in NOD/SCID/β2m^{null} mice (*bottom left and right*; *bar,* 300 and 100 μm, respectively). *Right,* Kaplan-Meier curve illustrates the *in vivo* survival data. *C,* by immunohistochemistry, we have characterized the s.c. tumors using three different epithelial specific markers, AE1/AE3, CK18, and CK13 (*left*, from top; *bar,* 100 μm), as well as the primitive/mesenchymal marker vimentin, the myogenous differentiation marker actin 1A4, and CD99, a marker of primitive neuroectodermal tumors and Ewing sarcoma (*right*, from top; *bar,* 100 μm). *D,* fluorescence *in situ* hybridization analysis using a human specific probe (green) and a mice specific probe (*red*) show tumor-host interactions (*top, arrows*) and tumor vessel formation established by the host cells (*bottom*). *Bar,* 50 μm.

in many immortal cell lines, but the majority of normal somatic cells do not present any detectable telomerase activity. In accordance with published literature on hMSC (32–34), our telomerase activity assay confirmed the low endogenous levels of telomerase activity in hMSC (Fig. 3). Following malignant transformation, the telomerase activity increased significantly (P = 0.00003), in agreement with previous reports on malignant transformation (11, 22).

Enhanced anchorage-independent growth of TMC. Parallel to the observation of altered morphology and proliferation rate, we observed enhanced anchorage-independent growth and colony formation of TMC in soft agar assays, indicating malignant transformation (Fig. 4). The hMSC did not show colony formation in soft agar assays.

TMC are tumorigenic *in vivo*. To evaluate the tumorigenicity of TMC *in vivo*, cells were transduced with lentiviral eGFP vectors and injected i.v. into NOD/SCID/$\beta 2m^{null}$ mice. Engraftment of i.v. injected TMC-eGFP and subsequent disease progression were monitored longitudinally by time-domain optical imaging of eGFP fluorescence. We observed initial colonization by TMC-eGFP of the lungs from day 9, a finding subsequently confirmed by *ex vivo* optical imaging of the different organs at necropsy (Fig. 5*A*). All of the animals injected with TMC were euthanized within 39 days postinjection due to symptoms related to tumor burden (Fig. 5*B*, Kaplan-Meier curve). Control animals injected with hMSC were sacrificed 3 months postinjection without signs of tumor development.

For histolopathologic examination, TMC or TMC-LacZ were injected i.v. or s.c. into NOD/SCID mice. TMC-LacZ injected i.v. initiated tumor formation in the lungs (Fig. 5*B, bottom*, H&E sections). The TMC tumor tissue exhibited epitheloid characteristics by means of polygonal tumor cells arranged in solid clusters and high vascularity (Fig. 5*B, top*, H&E sections). By immunohistochemistry, we have characterized the s.c. tumors using three epithelial specific markers, AE1/AE3 (a cytokeratin cocktail), CK18, and CK13 (Fig. 5*C, left*), as well as the primitive/mesenchymal marker vimentin, a marker of myogenous differentiation (actin 1A4), and a marker of desmoplastic small round blue cell tumors and Ewing sarcoma (CD99; Fig. 5*C, right*). Taken together, these results indicate that the TMC give rise to morphologically epitheloid tumors with expression of epithelial and mesenchymal markers of differentiation. Staining with human and mouse specific centromere probes verified the human origin of the tumor (Fig. 5*D*), and showed involvement of host endothelial cells in neovascularization in developing s.c. tumors (Fig. 5*D, bottom*).

Recent publications present conflicting evidence about the transformation propensity of hMSC. Whereas Rubio and colleagues (11) observed spontaneous malignant transformation of adipose-derived hMSC *in vitro*, other investigators reported hMSC to remain stable with no transformation in long-term cultures of bone marrow– and adipose tissue–derived hMSC (9, 10). In line with the findings of Rubio and colleagues, we have shown that TMC depend on high hTERT expression to sustain the telomerase activity required for their rapid proliferation. According to several reports, the telomerase *hTERT* gene alone does not induce malignant transformation (33, 35). However, in a recent study, Christensen and colleagues (36) show that *hTERT*-transduced hMSC are prone to extensive radiation-induced genomic instability and subsequent malignant transformation. One possibility is that *in vitro* cell culture conditions provide stress-induced genomic instability, contributing to the malignant phenotype. Notably, mutation propensity has been related to oxygen tension (37), and matrix elasticity reported to direct lineage specificity of MSC in culture (38, 39). Thus, optimalization of *ex vivo* culture conditions is a prerequisite for expansion of hMSC for use in clinical protocols. Whatever the complete mechanism of spontaneous malignant transformation may be, the findings of our laboratories highlight the unstable nature of undifferentiated bone marrow–derived hMSC and the need to determine the molecular pathways involved in spontaneous transformation before safe use in clinical protocols.

In a larger context, our data fit into a scenario in which hMSC *in vivo* home from their areas of residence into areas of inflammation or extensive tissue damage to contribute to tissue repair and restoration of tissue homeostasis. Areas of recurrent or continuous repair are prone to malignant transformation, and hMSC may ultimately contribute to the development of cancer *in situ* as shown by others. Although such processes most likely are tightly controlled, there may be instances where an inflammatory microenvironment as a stress factor could trigger genetic events that favor malignant transformation.

Conclusions

Our results show that a significant fraction of bone marrow–derived hMSC samples undergo spontaneous malignant transformation following *in vitro* culture. In our opinion, this has a tremendous effect on the biosafety issues of future cell-based therapies and regenerative medicine regimens.

Disclosure of Potential Conflicts of Interest

No potential conflicts of interest were disclosed.

Acknowledgments

Received 12/8/08; revised 4/15/09; accepted 5/1/09; published OnlineFirst 6/9/09.

Grant support: Norwegian Cancer Society, The Norwegian Research Council, The Innovest Program on Quality Research, Helse-Vest, Haukeland University Hospital, The Bergen Translational Research Program, the Centre de Recherche de Public de la Santé (CRP-Santé) through a grant from the Research Ministry in Luxembourg, the European Commission 6th Framework Programme (contract 504743), and the Binational SYSTHER-INREMOS Virtual Institute, funded by the German and Slovenian Federal Ministries of Education and Research. The funding by the Wilhelm-Toennis Grant of the German Society of Neurosurgery is appreciated.

The costs of publication of this article were defrayed in part by the payment of page charges. This article must therefore be hereby marked *advertisement* in accordance with 18 U.S.C. Section 1734 solely to indicate this fact.

We thank Christine Eriksen and Synnøve Yndestad for technical assistance, and Ole Johnny Steffensen for immunohistochemical staining. Furthermore, we would like to thank the volunteer bone marrow donors, who made this study possible.

References

1. Woodbury D, Schwarz EJ, Prockop DJ, Black IB. Adult rat and human bone marrow stromal cells differentiate into neurons. J Neurosci Res 2000;61:364–70.
2. Arthur A, Zannettino A, Gronthos S. The therapeutic applications of multipotential mesenchymal/stromal stem cells in skeletal tissue repair. J Cell Physiol 2009; 218:237–45.
3. Studeny M, Marini FC, Dembinski JL, et al. Mesenchymal stem cells: potential precursors for tumor stroma and targeted-delivery vehicles for anticancer agents. J Natl Cancer Inst 2004;96:1593–603.
4. Zhang X, Nakaoka T, Nishishita T, et al. Efficient adeno-associated virus-mediated gene expression in human placenta-derived mesenchymal cells. Microbiol Immunol 2003;47:109–16.
5. Tsai MS, Lee JL, Chang YJ, Hwang SM. Isolation of human multipotent mesenchymal stem cells from second-trimester amniotic fluid using a novel two-stage culture protocol. Hum Reprod 2004;19:1450–6.

6. Bieback K, Kluter H. Mesenchymal stromal cells from umbilical cord blood. Curr Stem Cell Res Ther 2007;2:310–23.
7. Zuk PA, Zhu M, Ashjian P, et al. Human adipose tissue is a source of multipotent stem cells. Mol Biol Cell 2002;13:4279–95.
8. Le Blanc K, Pittenger M. Mesenchymal stem cells: progress toward promise. Cytotherapy 2005;7:36–45.
9. Bernardo ME, Zaffaroni N, Novara F, et al. Human bone marrow derived mesenchymal stem cells do not undergo transformation after long-term *in vitro* culture and do not exhibit telomere maintenance mechanisms. Cancer Res 2007;67:9142–9.
10. Meza-Zepeda LA, Noer A, Dahl JA, Micci F, Myklebost O, Collas P. High-resolution analysis of genetic stability of human adipose tissue stem cells cultured to senescence. J Cell Mol Med 2008;12:553–63.
11. Rubio D, Garcia-Castro J, Martin MC, et al. Spontaneous human adult stem cell transformation. Cancer Res 2005;65:3035–9.
12. Wang Y, Huso DL, Harrington J, et al. Outgrowth of a transformed cell population derived from normal human BM mesenchymal stem cell culture. Cytotherapy 2005;7:509–19.
13. Lapidot T, Sirard C, Vormoor J, et al. A cell initiating human acute myeloid leukaemia after transplantation into SCID mice. Nature 1994;367:645–8.
14. Al-Hajj M, Wicha MS, Benito-Hernandez A, Morrison SJ, Clarke MF. Prospective identification of tumorigenic breast cancer cells. Proc Natl Acad Sci U S A 2003;100:3983–8.
15. Li C, Heidt DG, Dalerba P, et al. Identification of pancreatic cancer stem cells. Cancer Res 2007;67:1030–7.
16. Singh SK, Hawkins C, Clarke ID, et al. Identification of human brain tumour initiating cells. Nature 2004;432:396–401.
17. Takaishi S, Okumura T, Wang TC. Gastric cancer stem cells. J Clin Oncol 2008;26:2876–82.
18. Tysnes BB, Bjerkvig R. Cancer initiation and progression: involvement of stem cells and the microenvironment. Biochim Biophys Acta 2007;1775:283–97.
19. Gibbs CP, Kukekov VG, Reith JD, et al. Stem-like cells in bone sarcomas: implications for tumorigenesis. Neoplasia 2005;7:967–76.
20. Houghton J, Stoicov C, Nomura S, et al. Gastric cancer originating from bone marrow-derived cells. Science 2004;306:1568–71.
21. Li H, Fan X, Kovi RC, et al. Spontaneous expression of embryonic factors and p53 point mutations in aged mesenchymal stem cells: a model of age-related tumorigenesis in mice. Cancer Res 2007;67:10889–98.
22. Miura M, Miura Y, Padilla-Nash HM, et al. Accumulated chromosomal instability in murine bone marrow mesenchymal stem cells leads to malignant transformation. Stem Cells 2006;24:1095–103.
23. Schichor C, Birnbaum T, Etminan N, et al. Vascular endothelial growth factor A contributes to glioma-induced migration of human marrow stromal cells (hMSC). Exp Neurol 2006;199:301–10.
24. Meyerrose T, Rosova I, Dao M, Herrbrich P, Bauer G, Noltak J. Establishment and transduction of primary human stromal/mesenchymal stem cell monolayers. In: Nolta JA, editor. Genetic engineering of mesenchymal stem cells. Dordrecht (The Netherlands): Springer 2005.
25. Stute N, Holtz K, Bubenheim M, Lange C, Blake F, Zander AR. Autologous serum for isolation and expansion of human mesenchymal stem cells for clinical use. Exp Hematol 2004;32:1212–25.
26. Joo A, Aburatani H, Morii E, Iba H, Yoshimura A. STAT3 and MITF cooperatively induce cellular transformation through upregulation of c-fos expression. Oncogene 2004;23:726–34.
27. Kollet O, Peled A, Byk T, et al. β2 microglobulin-deficient (B2m(null)) NOD/SCID mice are excellent recipients for studying human stem cell function. Blood 2000;95:3102–5.
28. McCormack E, Micklem DR, Pindard LE, et al. *In vivo* optical imaging of acute myeloid leukemia by green fluorescent protein: time-domain autofluorescence decoupling, fluorophore quantification, and localization. Mol Imaging 2007;6:193–204.
29. Conget PA, Minguell JJ. Phenotypical and functional properties of human bone marrow mesenchymal progenitor cells. J Cell Physiol 1999;181:67–73.
30. Deans RJ, Moseley AB. Mesenchymal stem cells: biology and potential clinical uses. Exp Hematol 2000;28:875–84.
31. Shay JW, Wright WE. Hallmarks of telomeres in ageing research. J Pathol 2007;211:114–23.
32. Parsch D, Fellenberg J, Brummendorf TH, Eschlbeck AM, Richter W. Telomere length and telomerase activity during expansion and differentiation of human mesenchymal stem cells and chondrocytes. J Mol Med 2004;82:49–55.
33. Simonsen JL, Rosada C, Serakinci N, et al. Telomerase expression extends the proliferative life-span and maintains the osteogenic potential of human bone marrow stromal cells. Nat Biotechnol 2002;20:592–6.
34. Zimmermann S, Voss M, Kaiser S, Kapp U, Waller CF, Martens UM. Lack of telomerase activity in human mesenchymal stem cells. Leukemia 2003;17:1146–9.
35. Burger AM, Fiebig HH, Kuettel MR, Lautenberger JA, Kung HF, Rhim JS. Effect of oncogene expression on telomerase activation and telomere length in human endothelial, fibroblast and prostate epithelial cells. Int J Oncol 1998;13:1043–8.
36. Christensen R, Alsner J, Brandt Sorensen F, Dagnaes-Hansen F, Kolvraa S, Serakinci N. Transformation of human mesenchymal stem cells in radiation carcinogenesis: long-term effect of ionizing radiation. Regen Med 2008;3:849–61.
37. Busuttil RA, Rubio M, Dolle ME, Campisi J, Vijg J. Oxygen accelerates the accumulation of mutations during the senescence and immortalization of murine cells in culture. Aging Cell 2003;2:287–94.
38. Engler AJ, Sen S, Sweeney HL, Discher DE. Matrix elasticity directs stem cell lineage specification. Cell 2006;126:677–89.
39. Rowlands AS, George PA, Cooper-White JJ. Directing osteogenic and myogenic differentiation of MSCs: interplay of stiffness and adhesive ligand presentation. Am J Physiol Cell Physiol 2008;295:C1037–44.
40. Woodfin A, Voisin MB, Nourshargh S. PECAM-1: a multi-functional molecule in inflammation and vascular biology. Arterioscler Thromb Vasc Biol 2007;27:2514–23.
41. Nielsen JS, McNagny KM. Novel functions of the CD34 family. J Cell Sci 2008;121:3683–92.
42. Naor D, Sionov RV, Ish-Shalom D. CD44: structure, function, and association with the malignant process. Adv Cancer Res 1997;71:241–319.
43. Alexander DR. The CD45 tyrosine phosphatase: a positive and negative regulator of immune cell function. Semin Immunol 2000;12:349–59.
44. Haynesworth SE, Baber MA, Caplan AI. Cell surface antigens on human marrow-derived mesenchymal cells are detected by monoclonal antibodies. Bone 1992;13:69–80.
45. Rege TA, Hagood JS. Thy-1, a versatile modulator of signaling affecting cellular adhesion, proliferation, survival, and cytokine/growth factor responses. Biochim Biophys Acta 2006;1763:991–9.
46. Fonsatti E, Del Vecchio L, Altomonte M, et al. Endoglin: an accessory component of the TGF-β-binding receptor-complex with diagnostic, prognostic, and bioimmunotherapeutic potential in human malignancies. J Cell Physiol 2001;188:1–7.
47. van Kempen LC, Nelissen JM, Degen WG, et al. Molecular basis for the homophilic activated leukocyte cell adhesion molecule (ALCAM)-ALCAM interaction. J Biol Chem 2001;276:25783–90.
48. Simmons PJ, Torok-Storb B. Identification of stromal cell precursors in human bone marrow by a novel monoclonal antibody, STRO-1. Blood 1991;78:55–62.
49. Spector M. Musculoskeletal connective tissue cells with muscle: expression of muscle actin in and contraction of fibroblasts, chondrocytes, and osteoblasts. Wound Repair Regen 2001;9:11–8.
50. Choo SY. The HLA system: genetics, immunology, clinical testing, and clinical implications. Yonsei Med J 2007;48:11–23.